Imaging Intramolecular Coulomb Repulsions in Multiply Charged Anions

Xiao-Peng Xing, Xue-Bin Wang, and Lai-Sheng Wang*

Department of Physics, Washington State University, 2710 University Drive, Richland, Washington 99354, USA and Chemical and Materials Sciences Division, Pacific Northwest National Laboratory, MS K8-88, Richland, Washington 99352, USA

(Received 7 June 2008; published 21 August 2008)

The properties of multiply charged anions are dominated by intramolecular Coulomb repulsion (ICR). Using photoelectron imaging, we show the effect of ICR on photoelectron angular distributions for a series of dianions, $^{-}O_2C(CH_2)_nCO_2^{-}$ (D_n^{2-}). The observed photoemission band of D_n^{2-} was due to a perpendicular transition from the charged end group. However, photoemission intensities were observed to peak along the laser polarization for smaller n due to the strong ICR that forces electrons to be emitted along the molecular axis. This emission pattern weakens with increasing n and at D_{11}^{2-} the angular distribution reverses back to peak at the perpendicular direction due to the reduced ICR.

DOI: 10.1103/PhysRevLett.101.083003 PACS numbers: 33.80.Eh, 36.90.+f

Free multiply charged anions (MCAs) are exotic molecular and electronic systems and their properties are strongly influenced by intramolecular Coulomb repulsions, which make most textbook MCAs unstable in the isolated state [1,2]. Thus, despite their prevalence in the condensed phase, MCAs were rarely observed in the gas phase [3–6]. However, the electrospray ionization technique, invented by Fenn as a soft ionization method for biological mass spectrometry [7], has proven to be ideal to transport MCAs from solution samples to the gas phase and has allowed rapid recent experimental progresses in the study of free MCAs in the past decade [8–15]. A major advance in the study of MCAs was achieved by the coupling of electrospray with photoelectron spectroscopy (PES) [9,11,16], which has been shown to be a powerful technique to probe the intrinsic stability and electronic structure of MCAs [11,17–19]. The repulsive Coulomb barrier universally present in MCAs was directly observed by PES [9,17], as well as negative electron binding energies [20], which exist in long-lived metastable MCAs. PES of MCAs is expected to exhibit interesting angular distributions due to the strong intramolecular Coulomb repulsion which should determine the preferred directions of photoemission. However, up to now no angle-resolved PES has been done on MCAs. Here we report photoelectron imaging on a series of doubly charged anions, $^{-}O_2C(CH_2)_nCO_2^{-}$ ($n = 3$–11), yielding photoemission angular distributions and allowing intramolecular Coulomb repulsion to be directly imaged.

The imaging method was developed to record spatial distributions of photodissociation products [21], or photoelectrons produced from multiphoton ionization of Xe [22], by projecting the expanding photoproducts from the interaction zone onto a two-dimensional position-sensitive detector. Photoelectron imaging was soon applied to small W_n^- cluster anions because of its high sensitivity to low energy electrons [23], as well as CF_3^- [24]. With the development of the velocity-map imaging technique [25], photoelectron imaging has evolved into a powerful alternative PES method over the past several years [26,27]. A key advantage of photoelectron imaging lies at its high detection efficiency while yielding angular distributions at the same time. In particular, its high sensitivity to low energy electrons has led to high resolution spectroscopy, comparable to zero electron-kinetic-energy PES, using the slow electron velocity-map imaging mode [28].

The current study was carried out on our electrospray PES apparatus [16] by replacing the original magnetic-bottle photoelectron analyzer with a velocity-map imaging system, constructed according to Eppink and Parker [25]. The dicarboxylate dianions, $^{-}O_2C(CH_2)_nCO_2^{-}$ ($n = 3$–11), were produced via electrospray of the respective salt solutions at ~1 mM concentration in a mixed water-methanol solvent, as described previously [17]. Each dianion of interest was mass selected and directed into the center of the photoelectron imaging lens system, where they were detached by a linearly polarized laser beam (355 nm, 3.496 eV) from a Nd:YAG laser (typical laser flux used was 4.5 mJ/cm^2). The nascent electron cloud was accelerated by a high voltage pulse applied to the imaging electrode and was projected onto a phosphor screen behind a set of microchannel plates. The positions of the photoelectrons on the phosphor screen were recorded by a CCD camera and accumulated as a photoelectron image. The usual accumulation time was about 10^5 laser shots at a 10 Hz repetition rate. The electron kinetic energy (KE) resolution ($\Delta KE/KE$) ranges from 3.7% for low energy electrons to better than 3% for electrons above 1 eV, as calibrated from the 355 nm spectra of Br^-, I^-, and ClO_2^-. This resolution was comparable to our previous magnetic-bottle apparatus [16].

Figure 1 displays the raw photoelectron images of $^{-}O_2C(CH_2)_nCO_2^{-}$ (or D_n^{2-} for short) ($n = 3$–11) at 355 nm. These dianions were studied previously using the magnetic-bottle apparatus [17]. At 355 nm, only the first detachment band could be accessed, corresponding to the outer ring observed in Fig. 1. The photoelectron veloc-

 © 2008 The American Physical Society

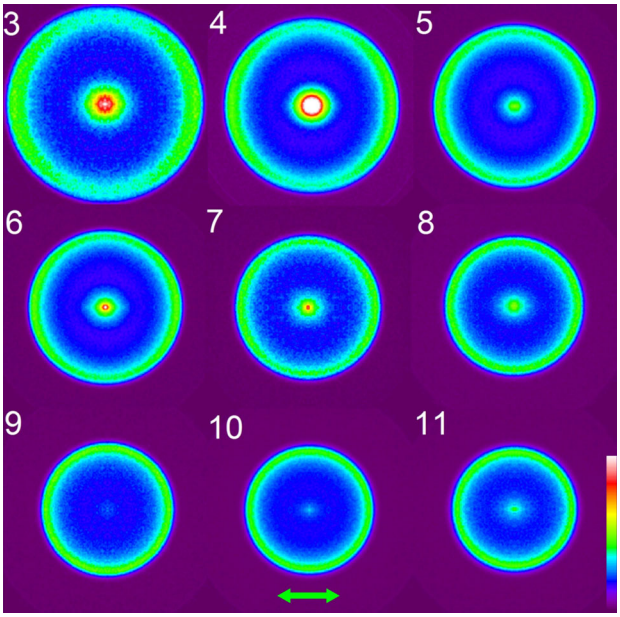

FIG. 1 (color online). Photoelectron images of dicarboxylate dianions, $^{-}O_2C(CH_2)_nCO_2^{-}$ (D_n^{2-}) ($n = 3$–11) at 355 nm (3.496 eV). The scale bar is in the right-hand bottom corner. The double arrow on the bottom indicates the directions of the laser polarization.

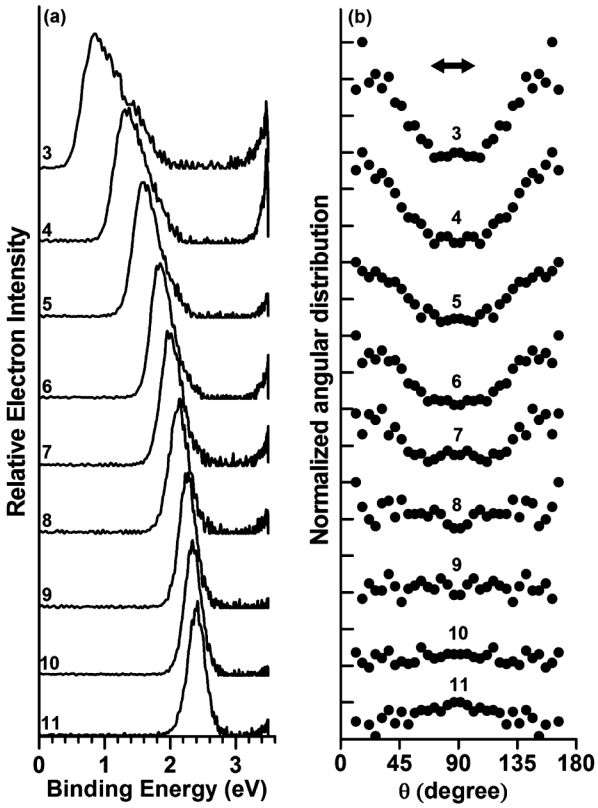

FIG. 2. (a) Photoelectron spectra of $^{-}O_2C(CH_2)_nCO_2^{-}$ ($n = 3$–11) obtained from the images in Fig. 1. The photoelectron kinetic energy is obtained from the radius (R) of the image, KE $\propto R^2$, calibrated by the photoelectron images of Br^- and I^-. The photoelectron intensity is obtained by integrating all angles from the images after inverse Abel transformation. (b) Photoelectron angular distributions normalized to one for the maximum intensity in each frame. The vertical scale is 0.1 per tick [see Fig. 4(b)]. Because of symmetry, only the top half of the image from Fig. 1 is plotted from 0° to 180°. The double arrow represents the directions of the laser polarization.

ity is proportional to the radius of the ring, and the decreasing radius from D_3^{2-} to D_{11}^{2-} indicates the decreasing electron kinetic energies or increasing electron binding energies, as the chain length increases. The central spot corresponds to near threshold electrons, which could come from either the product monoanion upon absorption of a second photon or other photoprocesses of the parent dianion, such as thermionic emission. The most interesting observation is the anisotropy (or angular distribution) in the outer ring in the PES images: it is strongly peaked along the laser polarization direction, in particular at smaller n. This anisotropy seems to weaken as the size of the dianion increases, and near isotropic electron distributions are observed for $n > 8$. In fact, the image of D_{11}^{2-} displays hints that the photoelectrons peak in the perpendicular direction, opposite to the trend in the smaller dianions.

Figure 2(a) shows the PES spectra in binding energies obtained from the images in Fig. 1 after inverse Abel transformations [29] and by integrating electron signals at all angles. These spectra look identical to those measured previously using the magnetic-bottle apparatus [17]. Figure 2(b) shows the photoelectron angular distributions, normalized to one as the maximum intensity. Figure 2(b) is essentially a numerical representation of the anisotropies revealed by the images in Fig. 1 (only the top half of the ring from 0° to 180°). The peaks along the laser polarization ($\theta = 0°$ and 180°) and the minimum perpendicular to the laser polarization ($\theta = 90°$) are clearly shown in the smaller dianions from $n = 3$–8. The peaking along the laser polarization gradually weakens with increasing n and the electron distribution becomes essentially isotropic for $n = 9$ and 10. At $n = 11$, the distribution starts to peak at $\theta = 90°$, completely opposite to the behavior in the smaller dianions. As shown previously [17], the first PES band for D_n^{2-} came from detachment of an O lone-pair electron from the terminal carboxylate group, which is identical for all the D_n^{2-} dianions independent of the chain length. The question is, What causes the change of the photoelectron angular distributions from $n = 3$ to 11?

The gradual trend of the electron angular distributions as a function of chain length suggests that the peaks in the directions along the laser polarization are caused by intramolecular Coulomb repulsion in the smaller D_n^{2-} dianions. As the chain length increases, intramolecular Coulomb repulsion decreases, leading to a reduction in the peaking along the laser polarization. Hence, the electron distributions become more and more isotropic from $n = 3$ to 8 and they become completely isotropic for $n = 9$

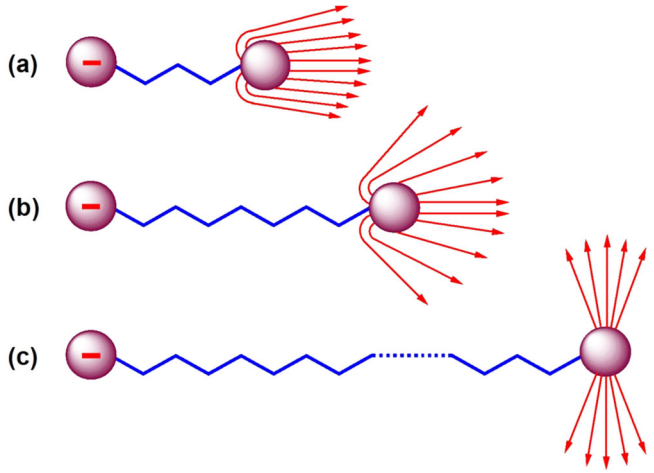

FIG. 3 (color online). Schematics illustrating the trajectories for photoelectrons influenced by intramolecular Coulomb repulsion for the case of (a) a short chain D_3^{2-} dianion, (b) a longer chain D_7^{2-} dianion, and (c) an infinitively long chain D_∞^{2-}, where there is no intramolecular Coulomb repulsion.

and 10. And finally at $n = 11$, the electron distribution begins to peak at the perpendicular direction due to the much reduced intramolecular Coulomb repulsion (about 1 eV for $n = 11$ versus 2.6 eV for $n = 3$ [17]). Since the initial dianions are not oriented during the photodetachment, the observed trend suggests that there is a maximum in the detachment cross sections in the perpendicular direction when the dianions are aligned with the laser polarization, while the peaking along the laser polarization directions in the smaller dianions is entirely due to the strong intramolecular Coulomb repulsion, as schematically shown in Fig. 3. For an infinitively long chain D_∞^{2-} dianion, strong peaking should occur at $\theta = 90°$ [Fig. 3(c)]. In a finite sized D_n^{2-} dianion, a photoelectron emitted from one of the carboxylate end groups feels the Coulomb repulsion from the remaining charge, which directs the outgoing electron along the molecular axis [Figs. 3(a) and 3(b)]. For $n < 8$, the Coulomb repulsion is strong enough to create the maximum along the laser polarization, essentially reversing the original perpendicular transition to make it look like a parallel transition.

To confirm the above interpretations, we performed an experiment on a monocarboxylate, $CH_3CH_2CH_2CO_2^-$, which is equivalent to the case of D_∞^{2-}. The results are shown in Fig. 4. Because of the high electron binding energies of the monoanion, we used 266 nm in the photodetachment and observed two PES bands (X and A) [Fig. 4(a)]. The first band (X) should be similar to the first band of the D_n^{2-} dianions: the fact that the second band (A) was missing for D_n^{2-} in the 355 nm spectra was due to the repulsive Coulomb barrier, as discussed in detail previously [17]. Indeed, both the X and A bands for the monocarboxylate are perpendicular transitions, peaking strongly in the direction perpendicular to the laser polarization. This can be understood using symmetry analyses on the oxygen lone-pair electrons that give rise to these bands [30]. The anisotropy for the X band is shown more clearly in the angular distribution displayed in Fig. 4(b).

Within the dipole approximation, the angular distribution of photoelectrons for nonoriented molecules (neutral or singly charged) with linearly polarized light is described by [31]:

$$I(\theta) = c[1 + \beta P_2(\cos\theta)], \quad (1)$$

where θ is the angle between the laser electric field vector and the velocity vector of the photoelectron, $P_2(\cos\theta)$ is the second-order Legendre polynomial, β is the anisotropy parameter containing dynamical information of the photodetachment process, and c is a constant proportional to the total detachment cross section. In angle-resolved PES for neutral molecules or singly charged anions, the anisotropy parameter, which ranges from -1 for purely perpendicular transitions to $+2$ for purely parallel transitions, is usually

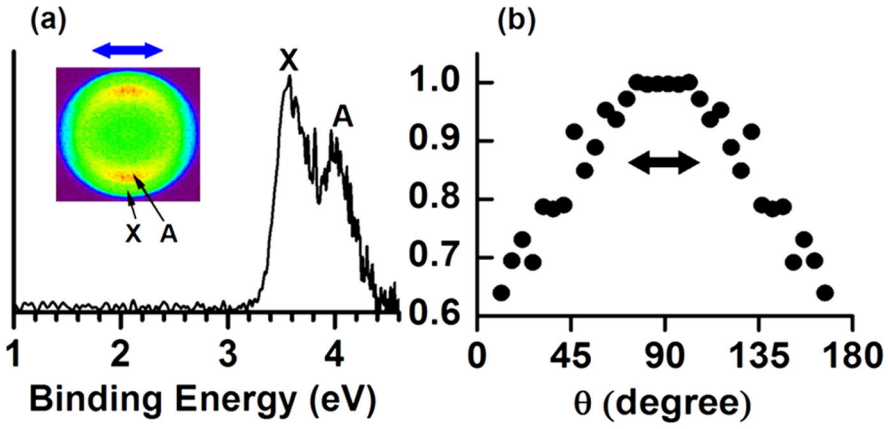

FIG. 4 (color online). Photoelectron imaging of $CH_3CH_2CH_2CO_2^-$ at 266 nm (4.661 eV). (a) Photoelectron spectrum obtained from the image showing in the inset (the color scale is the same as in Fig. 1). (b) Normalized photoelectron angular distribution for the X band [also see Fig. 2(b) caption). The arrows represent the laser polarization directions.

obtained, yielding information about the dynamics of the photodetachment process and the nature of the orbitals from which the electron is emitted. However, for MCAs Eq. (1) is no longer appropriate because the photoelectron angular distributions are governed by intramolecular Coulomb repulsion. Thus, photoelectron imaging can yield directly dynamical information about intramolecular Coulomb repulsion in MCAs.

In conclusion, we report the first photoelectron imaging of multiply charged anions and show that the photoelectron angular distributions are dominated by intramolecular Coulomb repulsions. Photoelectron imaging provides a new experimental method to probe properties of MCAs. There are many interesting questions the imaging method can address, such as the dependence of the angular distributions with electron kinetic energies and the anisotropy of the repulsive Coulomb barrier in MCAs. The imaging method may also provide direct structural, as well dynamical, information about multiply charged anions.

We thank Professor M. A. Johnson and his group for valuable discussions and help during the construction of the imaging analyzer. We also thank Professor H. Reisler for the BASEX program used for the inverse Abel transformation. This work was supported by the U.S. Department of Energy, Office of Basic Energy Sciences, Chemical Science Division and partly by NSF and performed at the W. R. Wiley Environmental Molecular Sciences Laboratory, a national scientific user facility sponsored by DOE's Office of Biological and Environmental Research and located at Pacific Northwest National Laboratory, which is operated for DOE by Battelle.

*Corresponding author.
ls.wang@pnl.gov

[1] A. I. Boldyrev, M. Gutowski, and J. Simons, Acc. Chem. Res. **29**, 497 (1996).
[2] M. K. Scheller, R. N. Compton, and L. S. Cederbaum, Science **270**, 1160 (1995).
[3] S. N. Schauer, P. Williams, and R. N. Compton, Phys. Rev. Lett. **65**, 625 (1990).
[4] J. Kalcher and A. F. Sax, Chem. Rev. **94**, 2291 (1994).
[5] G. R. Freeman and N. H. March, J. Phys. Chem. **100**, 4331 (1996).
[6] C. Yannouleas, U. Landman, A. Herlert, and L. Schweikhard, Phys. Rev. Lett. **86**, 2996 (2001).
[7] J. B. Fenn, Angew. Chem., Int. Ed. **42**, 3871 (2003).
[8] A. T. Blades and P. Kebarle, J. Am. Chem. Soc. **116**, 10 761 (1994).
[9] X. B. Wang, C. F. Ding, and L. S. Wang, Phys. Rev. Lett. **81**, 3351 (1998).
[10] A. A. Tuinman and R. N. Compton, J. Phys. Chem. A **102**, 9791 (1998).
[11] X. B. Wang and L. S. Wang, J. Phys. Chem. A **104**, 1978 (2000).
[12] J. Friedrich, S. Gilb, O. T. Ehrler, A. Behrendt, and M. M. Kappes, J. Chem. Phys. **117**, 2635 (2002).
[13] A. Dreuw and L. S. Cederbaum, Chem. Rev. **102**, 181 (2002).
[14] A. B. Nielsen, P. Hvelplund, B. Liu, S. B. Nielsen, and S. Tomita, J. Am. Chem. Soc. **125**, 9592 (2003).
[15] W. E. Boxford and C. E. H. Dessent, Phys. Chem. Chem. Phys. **8**, 5151 (2006).
[16] L. S. Wang, C. F. Ding, X. B. Wang, and S. E. Barlow, Rev. Sci. Instrum. **70**, 1957 (1999).
[17] L. S. Wang, C. F. Ding, X. B. Wang, and J. B. Nicholas, Phys. Rev. Lett. **81**, 2667 (1998).
[18] X. B. Wang, X. Yang, and L. S. Wang, Int. Rev. Phys. Chem. **21**, 473 (2002).
[19] O. T. Ehrler, J. M. Weber, F. Furche, and M. M. Kappes, Phys. Rev. Lett. **91**, 113006 (2003).
[20] X. B. Wang and L. S. Wang, Nature (London) **400**, 245 (1999).
[21] D. W. Chandler and P. L. Houston, J. Chem. Phys. **87**, 1445 (1987).
[22] H. Helm, N. Bjerre, D. J. Dyer, D. L. Huestis, and M. Saeed, Phys. Rev. Lett. **70**, 3221 (1993).
[23] J. C. Pinare, B. Baguenard, C. Bordas, and M. Broyer, Phys. Rev. Lett. **81**, 2225 (1998).
[24] H. J. Deyerl, L. S. Alconcel, and R. E. Continetti, J. Phys. Chem. A **105**, 552 (2001).
[25] A. T. J. B. Eppink and D. H. Parker, Rev. Sci. Instrum. **68**, 3477 (1997).
[26] E. Surber and A. Sanov, J. Chem. Phys. **116**, 5921 (2002).
[27] A. V. Davis, R. Wester, A. E. Bragg, and D. M. Neumark, J. Chem. Phys. **118**, 999 (2003).
[28] A. Osterwalder, M. J. Nee, J. Zhou, and D. M. Neumark, J. Chem. Phys. **121**, 6317 (2004).
[29] V. Dribinski, A. Ossadtchi, V. A. Mandelshtam, and H. Reisler, Rev. Sci. Instrum. **73**, 2634 (2002).
[30] Based on photoelectron spectra of HCO_2^- by E. H. Kim *et al.*, J. Chem. Phys. **103**, 7801 (1995) and $CH_3CO_2^-$ by X. B. Wang *et al.*, J. Phys. Chem. A **110**, 5047 (2006), the *X* band contains photoelectrons from two oxygen lone-pair orbitals of a_1 and b_2 symmetries. However, the ionization cross section for the a_1 orbital is very small and the *X* band is dominated by the b_2 orbital. This b_2 orbital is similar to that in the CS_2^- anion, which was observed to be a perpendicular transition by E. Surber *et al.*, J. Phys. Chem. A **107**, 8215 (2003) and was interpreted using the so-called "*s*-*p* model" by these authors.
[31] J. Cooper and R. N. Zare, J. Chem. Phys. **48**, 942 (1968).